

Non-isothermal crystallization kinetics of sucrose palmitate reinforced poly(lactic acid) bionanocomposites

Ravibabu Valapa¹ · Sameer Hussain² ·
Parmeswar Krishnan Iyer² · G. Pugazhenth¹ ·
Vimal Katiyar¹

Received: 29 January 2015 / Revised: 27 May 2015 / Accepted: 14 July 2015 /
Published online: 11 August 2015
© Springer-Verlag Berlin Heidelberg 2015

Abstract Poly(lactic acid) (PLA) bionanocomposites containing sucrose palmitate (SP), which is a non-toxic food additive, were prepared by a simple solution-casting approach. In the current work, the investigation of non-isothermal cold crystallization kinetics of PLA and PLA–SP bionanocomposites was performed using a differential scanning calorimeter under the dynamic heating regime of 2.5, 5, 7.5 and 10 °C/min. Avrami model was employed to study the effect of SP on cold crystallization kinetics of PLA. For PLA–SP bionanocomposites, Avrami coefficients obtained in the range of ~ 2.5 –4 and decreasing trend of the $t_{1/2}$ values indicated the faster crystallization mechanism in comparison to neat PLA. The nucleation and growth mechanism involved in the non-isothermal crystallization of PLA and PLA–SP bionanocomposites were further analyzed by Tobin model.

Electronic supplementary material The online version of this article (doi:[10.1007/s00289-015-1468-3](https://doi.org/10.1007/s00289-015-1468-3)) contains supplementary material, which is available to authorized users.

✉ G. Pugazhenth¹
pugal@iitg.ernet.in

✉ Vimal Katiyar
vkatiyar@iitg.ernet.in

Ravibabu Valapa
valaparavi@gmail.com

Sameer Hussain
h.sameer@iitg.ernet.in

Parmeswar Krishnan Iyer
pki@iitg.ernet.in

¹ Department of Chemical Engineering, Indian Institute of Technology Guwahati, Guwahati 781039, Assam, India

² Department of Chemistry, Indian Institute of Technology Guwahati, Guwahati 781039, Assam, India

Kissinger method has been employed to determine the crystallization activation energy (ΔE) for neat PLA and PLA–SP bionanocomposite. The nucleation as well as the growth of spherulites in neat PLA and PLA–SP bionanocomposites was observed using polarized optical microscopy. After incorporation of SP in the PLA matrix, an increase in the overall crystallization rate for PLA was reflected by the decline in the nucleation induction period and subsequent enhancement in the primary nucleation sites.

Keywords Sucrose palmitate · Poly(lactic acid) · Differential scanning calorimetry · Non-isothermal crystallization kinetics · Avrami model · Polarized optical microscopy

Introduction

In recent years, poly(lactic acid) (PLA), linear aliphatic polyester, received significant interest as a promising candidate to replace petrochemical-derived polymers owing to its biodegradability and biocompatibility [1–3]. In particular, PLA possesses significant potential in the industrial sector for packaging application because of the combination of various intrinsic properties such as high transparency and barrier properties in comparison with conventional polymers like polyethylene and polypropylene [4, 5]. However, a slow crystallization rate and low crystallinity nature exhibited by PLA indeed seriously restrict its broader application [6, 7]. Crystallinity is one of the critical parameters that affect the key properties (i.e., mechanical and gas barrier resistance) and can be tailored by heat treatment or by employing nanofillers to the polymers. In general, crystalline structures of PLA can be formed when it is quenched from melting state under isothermal or non-isothermal environment [8–11]. As the non-isothermal crystallization process is more realistic for practical applications, it becomes primarily important to assess the same quantitatively [12–14]. The process where the orientation of PLA chains and the formation of crystallite structures take place when PLA is cooled from melt or heated above its glass transition temperature is called as “melt crystallization” or “cold crystallization”, respectively. Although PLA is a slow crystallizing polymer, it has been explored that an efficient way to increase the crystallization rate is addition of reinforcement that can act as nucleating agent [13]. Therefore, significant efforts are devoted to enhance crystallization properties of PLA by incorporation of several nucleating agents such as carbon nanotubes [15, 16], silica [17, 18], clay [19, 20], cellulose nanocrystals [21, 22] and starch [23, 24]. To broaden the utilization of PLA in particular for food packaging applications, incorporation of eco-friendly and biocompatible nucleating agents for the design of PLA composite systems is desirable.

In view of this, non-toxic food additive, “sucrose palmitate” (SP), is considered for the fabrication of PLA composites [25, 26]. The novel filler “SP” exhibited excellent barrier ($\sim 69\%$ reduction) and ductility ($\sim 56\%$ improvement) properties as compared to neat PLA [25]. In addition to this, detailed investigation on the thermal degradation kinetics for PLA–SP bionanocomposites was reported in our

earlier work [26]. After incorporation of any filler (or additive) in the polymer matrix, investigating the crystallization behavior of the resultant composite systems becomes essential. This is because of the incorporated additives affecting the crystallization process of polymers via two ways. First, the additives can act as nucleating agents leading to an enhancement in crystallization temperature, which have a positive response on the crystallization characteristics. Second, additives can impede the movement and diffusion of molecular chains of polymer to the surface of the growing nucleus of crystallites in the composite system. This phenomenon may lead to a reduction in crystallization temperature, which has a negative response to the crystallization process [27]. Therefore, the current work is devoted to examine the influence of novel filler, “SP”, on the non-isothermal crystallization behavior of PLA.

Differential scanning calorimetry (DSC) is widely used as a device for evaluation of crystallization as well as melting behaviors of polymers and helps in the basal perception of the kinetics of crystallization process. Information regarding the crystallization parameters derived from kinetic analysis can be utilized for the proper design of composite materials with desirable characteristics for food packaging applications. The crystallization as well as melting behavior of PLA–SP bionanocomposites under the dynamic heating regime is examined using DSC analysis. In addition to this, detailed analysis of non-isothermal cold crystallization kinetics for PLA and PLA–SP composites is carried out in the current work. The Avrami model that describes the isothermal crystallization kinetics is modified for non-isothermal crystallization and applied to deal with the experimental data obtained by DSC analysis. Avrami exponent (n) also provides knowledge about the nucleation mechanism of PLA–SP bionanocomposites. The kinetic parameters, n and K calculated from the modified Avrami model, are further utilized to evaluate the crystallization rate parameter (CRP) for PLA–SP bionanocomposites. The crystallization activation energy (ΔE) for the migration of PLA molecular chains to the growing crystal front is obtained by Kissinger method. The effect of SP on the spherulite morphology of PLA and the nucleation induction period is directly visualized by polarized optical microscopy (POM) under isothermal crystallization temperature.

Experimental

Materials

Sucrose palmitate from Sisterna (Netherlands) is used as the filler material. PLA obtained from Nature Works[®]; grade 2003D is used as the polymer matrix. Heat distortion temperature, melt flow index (g per 10 min) at 260 °C and specific gravity for PLA is 55 °C, 6 and 1.24, respectively. Chloroform obtained from Merck is used as the solvent for preparing PLA–SP composites.

PLA and PLA–SP film preparation

A series of neat PLA and PLA–SP bionanocomposites with various concentrations of SP were fabricated by a simple solution-casting method as follows: ~0.95 g of PLA was weighed and mixed in 50 mL of chloroform. PLA granules suspended in chloroform were stirred for 2 h to dissolve the same completely. Sucrose palmitate (1, 3, 5 wt% with respect to PLA matrix) was dissolved in chloroform with continuous stirring for 1 h separately. Then, the chloroform solution containing dissolved SP was transferred into the PLA–chloroform mixture and stirred for 2 h. The PLA–SP composite solution was cast on Teflon petri plates and dried under ambient conditions for 24 h. The dried bionanocomposites were peeled off carefully from the petri plates. The resulting bionanocomposites were finally dried under vacuum for 12 h at 40 °C for complete removal of solvent and then stored in a desiccator to carry out differential calorimetric analysis. Here, all the compositions are designated as SP, PLA, PLA–SP-1, PLA–SP-3, and PLA–SP-5 for sucrose palmitate, polylactic acid, polylactic acid/sucrose palmitate 1 wt%, polylactic acid/sucrose palmitate 3 wt% and polylactic acid/sucrose palmitate 5 wt%, respectively.

Characterization

Thermal properties and crystallization behavior of PLA and PLA–SP bionanocomposites were studied using a differential scanning calorimeter (Mettler Toledo-1 series). Samples (10 ± 0.5 mg) were hermetically sealed in aluminum pans and heated from 25 to 180 °C at various heating rates of 2.5, 5, 7.5 and 10 °C/min in an inert atmosphere (N_2 flow, 50 mL/min). All the samples were first heated from 25 to 180 °C and held at this temperature for 5 min to eliminate the effect of thermal and processing history. Glass transition temperature (T_g), cold crystallization temperature (T_{cc}), the enthalpy change at T_{cc} (ΔH_{cc}), melting temperature (T_m) and the enthalpy of fusion at T_m (ΔH_m) of pure PLA and bionanocomposites were determined from the DSC thermograph during the second heating cycle.

The nucleation and spherulite growth in PLA and PLA–SP bionanocomposites were observed using Leica DM 2500P polarizing optical microscope fitted with a QICAM FAST1394 camera. The Linkam LTS420 temperature control stage was used to study the morphological changes of film at an isothermal crystallization temperature (120 °C). Film samples of PLA and PLA–SP bionanocomposites with a thickness of about 50 ± 5 μm were first melted at 180 °C for 5 min to eliminate thermal histories, and were transferred immediately to a temperature of 120 °C for isothermal crystallization. The micrographs of growing spherulites were pictorialized at a specific interval of time before impingement of spherulites took place.

Results and discussion

The glass transition, crystallization and melting behaviors of the PLA and PLA–SP composites are evaluated using DSC analysis. DSC second heating thermographs of neat PLA and PLA–SP bionanocomposites obtained at a heating rate of 5 °C/min

are shown in Fig. S1. It can be seen from Fig. S1 that the T_g values for PLA and PLA–SP bionanocomposites remain the same (~ 61 °C). This suggests that incorporated SP did not induce the PLA degradation by forming the short-chain fragments. In contrast, filler-induced PLA degradation due to reduced macromolecular interactions has been reported in the literature [28, 29]. In the present study, a slight positive effect on the crystallization behavior of the PLA after the incorporation of filler can be noticed from Table 1. It can be seen from the DSC curves that the cold crystallization temperature (T_{cc}) increases significantly by 6, 14, 14 °C for 1, 3, 5 wt% loading of SP, respectively, in comparison with neat PLA. The enhancement in T_{cc} is due to the fact that the addition of SP suppresses the diffusion rate leading to the slower migration of the polymer chains to the surface of the nucleus [3, 30]. This also indicates that the crystallization rate becomes slower than pure PLA, as both homogeneous and heterogeneous crystallization took place within the composites [30].

In the melting region of PLA, unimodal endothermic peak ($T_m = 149$ °C) is observed, indicating the presence of PLA in α -crystalline form [26, 28, 31, 32]. This endotherm reveals the melting of stable crystals of PLA formed due to the absence of the heterogeneous distribution of crystals. Another possible reason for this could be uniform crystal thickness, developed in PLA after the reinforcement of the novel filler, and it can be attributed by half width full length (HWFL) of melting endotherm [33]. It can be noticed from Fig. S1 that T_m only slightly shifts to the higher temperature side after addition of SP in PLA matrix compared with the neat PLA. This may be due to the fact that filler surface reduces the critical nucleus size required for the formation of a thick, stable nucleus in PLA. The decrease in nucleus size reflects a prominent nucleation effect in PLA after incorporation of the filler [33]. In addition to this, the shift in T_m reveals that the addition of SP did not lower the molecular weight of PLA. The current result indicates that the SP acts as a better nucleating agent by enhancing T_m . The reduction in the heat of fusion for melting peaks with respect to loading of SP (wt%) is also observed from DSC scans. The ΔH_{cc} and ΔH_m values of bionanocomposite obtained from DSC analysis provide insight into the interactions between PLA and SP [34]. A small increment in the ΔH_{cc} and ΔH_m for the PLA–SP-1 in comparison with other sample can be noticed from Table 1, representing the stable crystals of PLA formed during the crystallization process. With further SP loadings, ΔH_{cc} and ΔH_m gradually decrease due to the slower migration of PLA chains to the nucleus surface because of strong

Table 1 DSC results for PLA and PLA–SP bionanocomposites

S no.	Sample	T_g (°C)	T_{cc} (°C)	T_m (°C)	ΔH_{cc}	ΔH_m	% X_c
1	PLA	61	110	149	16.14	27.20	~ 12
2	PLA–SP-1	60	117	150	17.20	31.98	~ 16
3	PLA–SP-3	60	125	152	5.14	19.27	~ 15
4	PLA–SP-5	60	125	152	1.51	13.16	~ 12

hydrogen bonding, leading to decline in percentage crystallinity compared with 1 wt% loading of SP. DSC results reveal that there is a slight improvement in the crystallinity of the PLA after incorporation of SP.

Non-isothermal cold crystallization kinetics of PLA and PLA–SP composites

Figure 1 shows the non-isothermal crystallization and melting behaviors of neat PLA and PLA–SP bionanocomposites investigated by DSC at various heating rates (2.5, 5, 7.5, and 10). The curves show an exothermic cold crystallization peak at about 100–121 °C for neat PLA, and at 105–125 °C for PLA–SP bionanocomposites. The curves also present an endothermic peak related to melting at about 148–151 °C for neat PLA and PLA–SP bionanocomposites. It can be seen from Fig. 1 that crystallization temperatures (T_{cc}) shift gradually to the higher temperature side with respect to heating rates for both PLA and PLA–SP bionanocomposites. This indicates that PLA requires excess time for crystallization at a higher heating rate [shown in Fig. S2 (a)]. The phenomenon is related to the lower heat

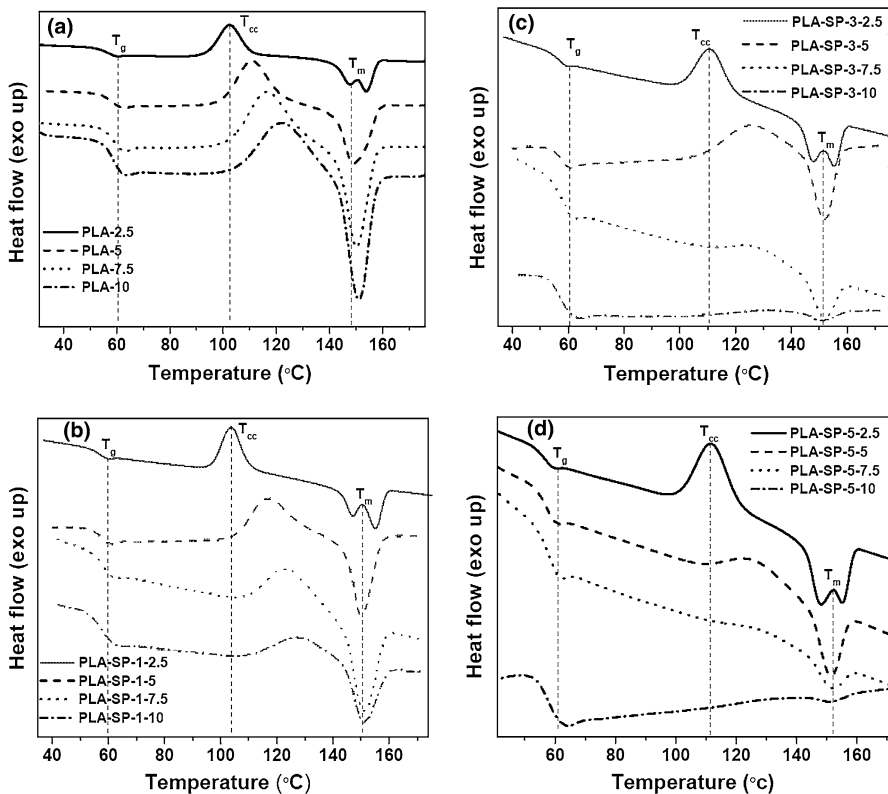


Fig. 1 DSC thermographs at different heating rates of 2.5, 5, 7.5 and 10 °C/min for **a** neat PLA, **b** PLA–SP-1, **c** PLA–SP-3 and **d** PLA–SP-5 bionanocomposites

transfer coefficient of the PLA, which delays crystallization with increasing heating rates [35]. For a lower heating rate (2.5 °C/min), two melting peaks for both PLA and PLA–SP composites can be observed. The melting peak that corresponds to the lower temperature is ascribed to the melting process of imperfect crystalline structures of PLA formed during the primary phase of the cold crystallization process. The higher temperature melting peak is attributed to the melting of the perfect crystalline structure of PLA formed at the later phase of the cold crystallization process as a result of increased thickness of lamellae [36–39]. In contrast, for a heating rate of 5 °C/min, the disappearance of the double melting peak is observed for both PLA and PLA–SP bionanocomposites. With the further increase in the heating rate, i.e., 10 °C/min, the cold crystallization peak of PLA and PLA–SP bionanocomposites becomes very small and hard to detect, indicating the formation of less perfect crystal structures due to faster heating process [35, 40]. The T_g values for all the samples with a constant heating rate remain similar, but the T_g for each material increases with the rise in the heating rate, owing to thermal delay [shown in Fig. S2(b)] [35, 40]. The enthalpy of cold crystallization (ΔH_{cc}) decreases for both PLA and PLA–SP composites with an increase of the heating rate. Because PLA molecular chains do not possess sufficient time to relax before the formation of crystal structures when subjected to faster heating process [35, 40]. The melting enthalpy (ΔH_m) also varies at a same pace as ΔH_{cc} , indicating that melting behaviors mainly arise due to melting of crystal structures formed during the cold crystallization process [35, 40].

The relative degree of crystallinity ($X(t)$), as a function of the crystallization time or temperature, is calculated from the crystallization exotherms of PLA and PLA–SP bionanocomposites by partial integration of the same. $X(t)$ as a function of temperature can be expressed by Eq. 1.

$$X(t) = \frac{\int_{T_0}^T \left(\frac{dH_c}{dT}\right) dT}{\int_{T_0}^{T_\infty} \left(\frac{dH_c}{dT}\right) dT} \quad (1)$$

where T_0 and T_∞ are temperatures that correspond to the onset and end of the crystallization process, respectively [41, 42]. In case of the non-isothermal cold crystallization process, crystallization time (t) and the corresponding temperature (T) can be related as follows:

$$t = \frac{T - T_0}{\phi} \quad (2)$$

where ϕ is the heating rate [41, 42]. The curves of relative crystallinity versus crystallization time for neat PLA and PLA–SP bionanocomposites are portrayed in Fig. 2. The relative crystallinity curves of both PLA and its bionanocomposites obtained at various heating rates exhibit sigmoidal shape characteristic curves, which are attributed to the impingement of spherulites at the later stage of the crystallization process [14, 43]. From these curves, the lag effects of heating rates

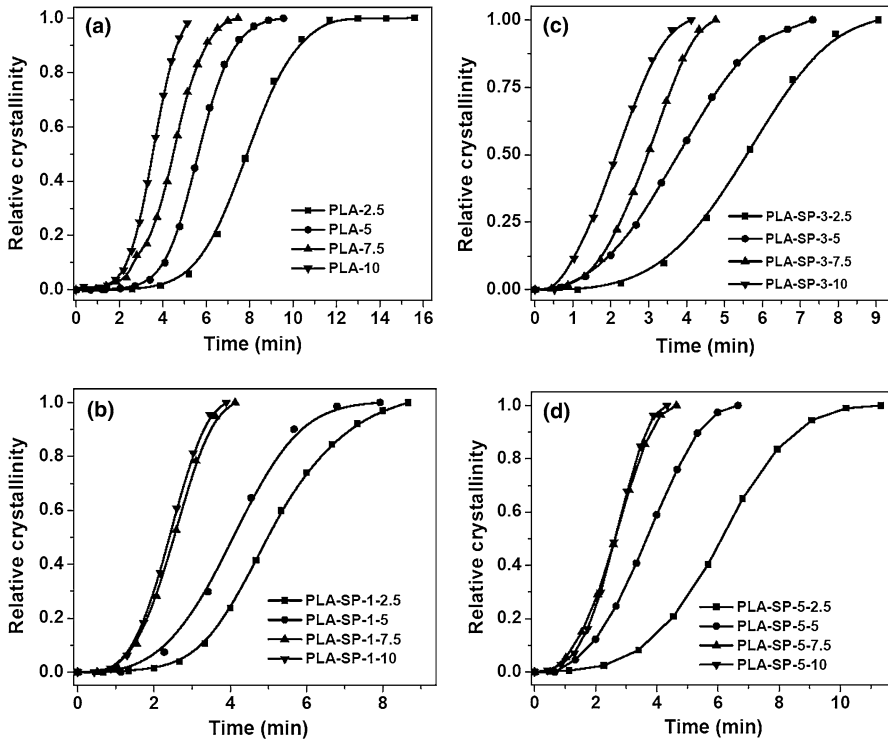


Fig. 2 Relative crystallinity versus crystallization time at different heating rates **a** neat PLA, **b** PLA–SP-1, **c** PLA–SP-3 and **d** PLA–SP-5 bionanocomposites

on crystallization process can be observed. Figure 2 also shows that at higher heating rates, PLA matrices have a shorter time of crystallization. This means that crystallization rates are increased with the incorporation of SP [35, 44].

The time required to achieve 50 % crystallization is called as half-time of crystallization ($t_{1/2}$) and is considered as a prime parameter for investigating the kinetics of crystallization process. The $t_{1/2}$ for non-isothermal crystallization can be obtained from the following expression [14, 35, 45]

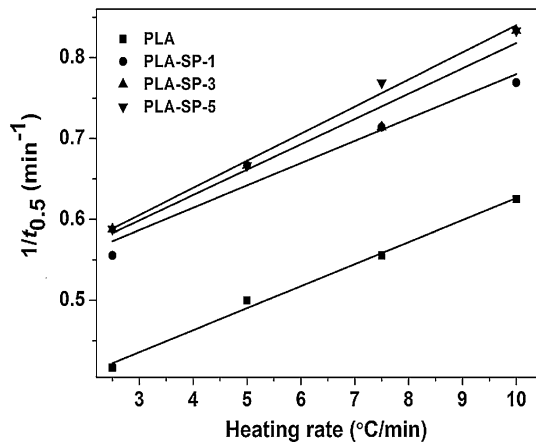
$$t_{1/2} = \left(\frac{\ln 2}{k} \right)^{1/n} \quad (3)$$

In general, shorter the $t_{1/2}$ values, faster will be the crystallization process. With increasing heating rate, the $t_{1/2}$ values for both PLA and its composites exhibit decreasing trends indicating shorter crystallization completion times. Moreover, the $t_{1/2}$ values for PLA–SP bionanocomposites are observed to be lower in comparison with neat PLA. This is due to the acceleration of the overall cold crystallization process after reinforcement of SP. However, the higher $t_{1/2}$ values observed for PLA and PLA–SP bionanocomposites at lower heating rates may be attributed to the

secondary crystallization process. The variation of $t_{1/2}$ with ϕ for neat PLA and its composites can be interpreted from Fig. 3. From the figure, the influence of ϕ and SP loading on overall crystallization rate of PLA bionanocomposites can be distinctly interpreted. It can be noticed that the $1/t_{1/2}$ value shoots up for PLA–SP bionanocomposites when compared to neat PLA. Hence, it becomes mandatory to discuss the effect of SP and its content (wt%) on the crystallization performance of PLA. Nucleation and growth are the two important aspects associated with the overall crystallization process of polymers [46]. The SP incorporated in the PLA matrix may engage in two distinct or contending functions influencing the crystallization process. On one hand, SP may involve in providing nucleation effect to fasten the non-isothermal crystallization process of PLA. On the other hand, there is a possibility that PLA chains will be present in an exceedingly intertwined during the melt state. Therefore, while due course of the crystallization process, PLA molecular segments must overwhelm definite energy barriers to migrate and bind onto the surface of the growing crystal front. The SP may serve as a cross-linking agent by obstructing the migration of PLA molecular fragments. This in turn hampers the growth of crystalline structures by restraining the nearby molecular segments of polymer during strong synergistic interactions exist between PLA and SP. There is a significant difference in the $1/t_{1/2}$ values between PLA and PLA–SP-1 bionanocomposite. This is due to the predominant nucleation effect induced by 1 wt% loading of SP enhancing the crystallization of PLA. However, further increase in the $1/t_{1/2}$ values for higher loadings of SP is not observed. Although SP might contribute in providing additional nucleation spots at higher loadings, the presence of more SP content may also create a much more appreciable detention consequence on the crystal growth process of PLA. Since the detention effect masks the nucleation effect, the overall crystallization rate is observed to be slow down at higher loadings of SP.

Zhang et al. [47, 48] introduced a method to evaluate the CRP, which describes the effect of filler on the crystallization rate of polymer quantitatively. Figure 3 shows the plot of $1/t_{1/2}$ versus ϕ for both the PLA and PLA bionanocomposites. The CRP is obtained from the slope of a linear plot of $1/t_{1/2}$ versus ϕ . The values of CRP

Fig. 3 Effect of SP loading on the CRP



are found to be 0.0272, 0.0276, 0.0313, and 0.0335 for PLA, PLA–SP-1, PLA–SP-3 and PLA–SP-5, respectively. The CRP values obtained for PLA–SP bionanocomposites point out that SP slightly enhances the cold crystallization of PLA matrix.

In the present work, the simplest kinetic model, “Avrami equation” is considered to determine the kinetic parameters associated with the non-isothermal crystallization process of PLA and is expressed by the following relationship:

$$X(t) = 1 - \exp(-kt^n) \quad (4)$$

The non-linear form of Eq. (4) is represented as

$$\log[-\ln(1 - X(t))] = \log k + n \log t \quad (5)$$

where $X(t)$ corresponds to relative crystallinity at time “ t ”, n refers to the Avrami exponent that defines the nucleation and crystal growth mechanisms, k represents the overall kinetic constant [49, 50]. The values of $\log[-\ln(1 - X(t))]$ are plotted as a function of $\log t$. Then, the Avrami exponent (n) and the crystallization rate constant (k) are obtained from the slope and intercept of the linear fit. A typical relative crystallinity curves for neat PLA, PLA–SP-1, PLA–SP-3 and PLA–SP-5 are shown in Fig. 2a–d and the corresponding Avrami plots for the same are presented in Fig. 4a–d. It can be noticed from Fig. 4a–d that good linearity is obtained for all the plots. This suggests that the theory seems to be helpful to appropriately elucidate the non-isothermal crystallization of PLA bionanocomposite systems.

In the current work, the n values (presented in Table 2) for neat PLA lie in the range of 4–5, which is in accordance with literature data [39, 40, 51]. This suggests that three-dimensional (3D) growth of PLA crystals takes place during the non-isothermal cold crystallization process and crystal growth is in disk-like nature by homogeneous nucleation. The n values for PLA–SP bionanocomposites are found in the range of ~ 2.5 –4, which is slightly lower in comparison with neat PLA. This is ascribed to the faster crystallization process that does not provide adequate time period for the crystals to grow in three dimensions, which in turn resulted in the heterogeneous nucleation process [39, 40, 51].

The Avrami model used for studying the crystallization kinetics of PLA and PLA–SP bionanocomposites is merely appropriate for investigating the early phase of crystallization process. This is due to that the Avrami model does not involve in describing the growth site impingement as well as secondary crystallization process. To investigate phase-transformation kinetics with growth site impingement in the non-isothermal crystallization kinetics of PLA and PLA–SP bionanocomposites, Tobin model is utilized, which is expressed by the following equation:

$$X_t = \frac{K_T t^{n_T}}{1 + K_T t^{n_T}} \quad (6)$$

where X_t , K_T and n_T correspond to the relative crystallinity at time ‘ t ’, Tobin crystallization rate constant and Tobin exponent, respectively [52]. The Tobin exponent (n_T) provides information about type of nucleation and growth mechanism involved in the non-isothermal crystallization process. The double logarithmic form of Eq. (6) is rewritten as:

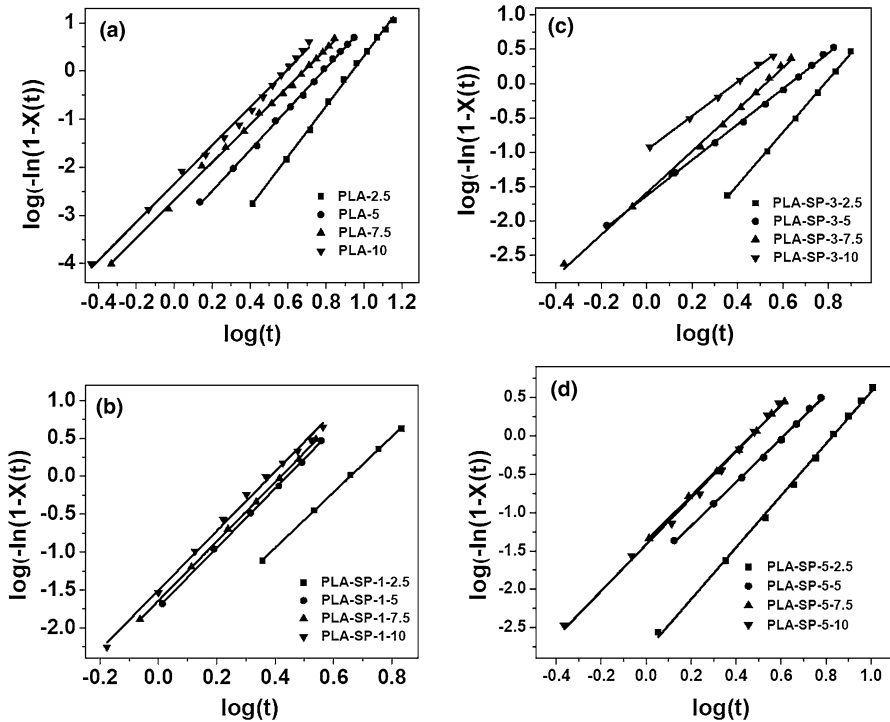


Fig. 4 Avrami plots for non-isothermal cold crystallization of **a** PLA, **b** PLA–SP-1, **c** PLA–SP-3 and **d** PLA–SP-5 bionanocomposites

Table 2 Avrami model parameters for PLA and PLA–SP bionanocomposites

S no.	Sample	<i>n</i>				log(<i>K</i>)			
		2.5 °C/ min	5 °C/ min	7.5 °C/ min	10 °C/ min	2.5 °C/ min	5 °C/ min	7.5 °C/ min	10 °C/ min
1	PLA	4.8	4.2	3.9	4	−4.9	−3.3	−2.6	−2.3
2	PLA–SP-1	3.9	3.9	3.9	3.7	−2.4	−1.7	−1.6	−1.5
3	PLA–SP-3	3.8	3.3	2.5	2.4	−3	−1.6	−1.5	−1.3
4	PLA–SP-5	3.8	3.5	2.9	2.7	−2.8	−1.7	−1.4	−1.3

$$\log\left(\frac{X_t}{1-X_t}\right) = \log K_T + n_T \log t \tag{7}$$

Tobin plots for PLA and PLA–SP bionanocomposites obtained for different heating rates are shown in Fig. 5a–d, in which $\log\left(\frac{X_t}{1-X_t}\right)$ is plotted against log

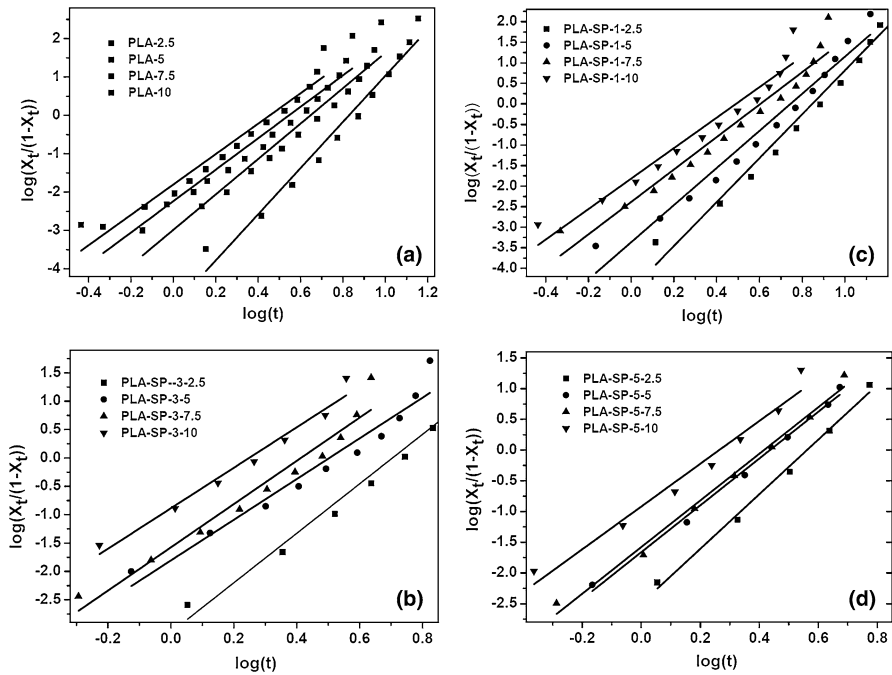


Fig. 5 Tobin plots for non-isothermal cold crystallization of **a** PLA, **b** PLA–SP-1, **c** PLA–SP-3 and **d** PLA–SP-5 bionanocomposites

t . Tobin parameters (n_T and K_T) are determined from the slope and intercept of the linear fit, respectively, and the same is summarized in Table 3.

It can be observed from Table 3 that the Tobin exponent ‘ n_T ’ value for PLA is in the range of 4–6. It decreases with respect to heating rate and the obtained value is comparable to the literature data [52]. Tobin parameter, K_T , exhibits increasing trend with an increase in the heating rate, which points out the faster crystallization process. In case of PLA–SP bionanocomposites, the ‘ n_T ’ values show decreasing trend with respect to heating rate. However, the values are found to be in the range of ~ 3 –5, which is relatively smaller in comparison to neat PLA, irrespective of the heating rate. This difference in the ‘ n_T ’ values suggests that the reinforcement of SP in the PLA matrix alters the crystallization process of PLA. It is also seen from Table 3 that the ‘ K_T ’ values obtained for PLA–SP bionanocomposites are higher when compared to neat PLA. This phenomenon indicates that the SP accelerates the non-isothermal crystallization process of PLA. The findings of the Tobin model discussed above are similar to the trend obtained for Avrami parameters. Hence, the Tobin parameters also describe the same physical significance analogous to that of Avrami model [53].

Table 3 Tobin model parameters for PLA and PLA–SP bionanocomposites

S no.	Sample	<i>n</i>				log(<i>K</i>)			
		2.5 °C/ min	5 °C/ min	7.5 °C/ min	10 °C/ min	2.5 °C/ min	5 °C/ min	7.5 °C/ min	10 °C/ min
1	PLA	6.0	4.6	4.1	3.9	−5.0	−3.0	−2.3	−1.9
2	PLA–SP-1	5.3	4.5	3.9	3.7	−4.5	−3.3	−2.2	−1.8
3	PLA–SP-3	4.3	3.6	3.8	3.5	−3.1	−1.8	−1.6	−1.3
4	PLA–SP-5	4.4	3.8	3.7	3.5	−2.5	−1.7	−1.6	−1.1

Crystallization activation energy of PLA and PLA–SP bionanocomposites

Kissinger method is used to determine the crystallization activation energy (ΔE) for non-isothermal cold crystallization of neat PLA and PLA–SP bionanocomposites. ΔE for the diffusion of the PLA segments to the surface of the growing crystal front is determined by calculating the variation of T_{cc} with respect to heating rate (ϕ) from the following expression:

$$\frac{d\left[\ln\left(\frac{\phi}{T_{cc}^2}\right)\right]}{d\left(\frac{1}{T_{cc}}\right)} = -\frac{\Delta E}{R} \quad (8)$$

where T_{cc} is the crystallization peak temperature, ΔE is the activation energy and R is the universal gas constant [35, 54]. Figure S3 shows the plots of $\ln\left(\phi \frac{d\alpha}{dT}\right)$ versus $\left(-\frac{1}{T}\right)$ for neat PLA and PLA–SP composites. The plots exhibit good linearity, and regression coefficients (R^2) values are obtained in the range of 0.9–0.999. ΔE obtained from the slopes of the linear plots shown in Fig. S3 is found to be 82, 67, 65, and 54 for PLA, PLA–SP-1, PLA–SP-3 and PLA–SP-5, respectively. ΔE values are found to decrease with respect to increase in SP loadings.

Polarized optical microscopy observations

The influence of SP as nucleation agent on the crystallization behavior of PLA matrix is perceived using a polarized optical microscope as shown in Fig. 6. PLA and PLA–SP bionanocomposites are heated up to 180 °C and the hot stage containing samples are maintained at the same temperature for a time span of 5 min to remove the thermal history. Optical micrographs are pictorialized in the 0th, 5th, 10th, 15th and 20th min at 120 °C after cooled from melt state at 180 °C for PLA and PLA–SP composites. In the current study, the process of nucleation and growth is controlling the overall crystallization kinetics of PLA. After incorporation of SP in the PLA matrix, an increase in the overall crystallization rate of PLA occurs. This is reflected through the diminution of the nucleation induction period followed by an increment in additional primary nucleation sites. For the PLA–SP

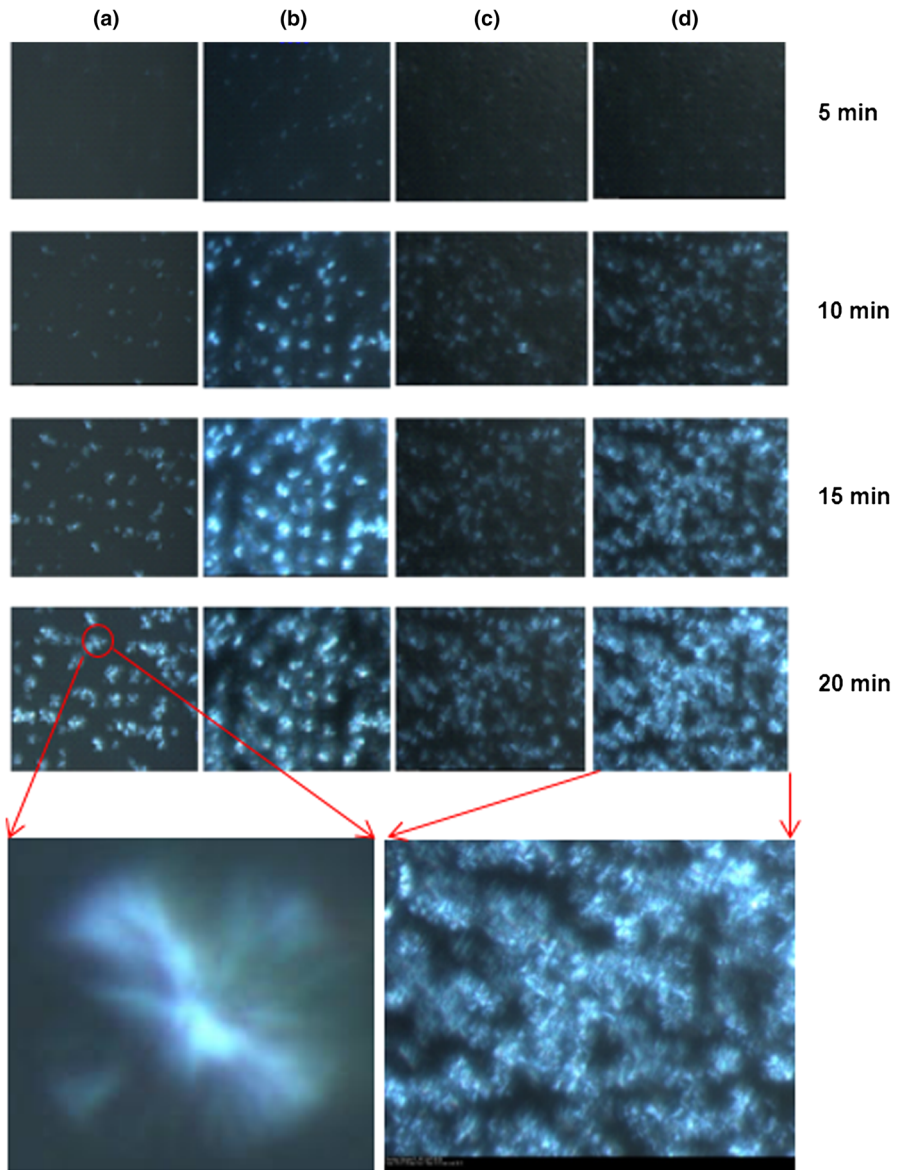
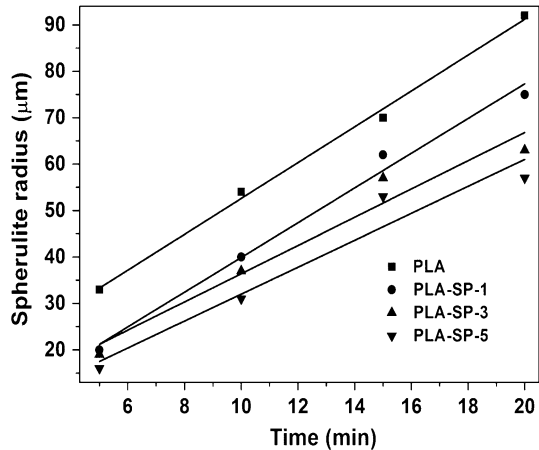


Fig. 6 Optical microscopy images of **a** PLA, **b** PLA-SP-1, **c** PLA-SP-3, and **d** PLA-SP-5 bionanocomposites with respect to time at 120 °C

bionanocomposites, the nucleation density of PLA spherulites is found to increase at 5, 10, 15 and 20 min in comparison with neat PLA. In addition to this, an appreciable increase in the nucleation density with respect to percentage weight loadings of SP is noticed, which indicate the better dispersion of SP in the PLA matrix. Therefore, more crystals have the ability to undergo nucleation and

Fig. 7 Variation of spherulite radius versus time



subsequently grow in the enhanced surface area of the interfaces owing to increment in the number of nucleating sites.

For neat PLA and PLA–SP composites, the radial spherulite growth rates are measured as a function of time. Figure 7 represents micrographs showing the change in spherulite radius over time at 120 °C. For both PLA and PLA–SP composites, the size of the spherulites amplifies linearly with respect to time. This conveys that the growth rate is not dependent on the spherulite diameter. In case, if it is considered that all the crystallizable species are not eliminated from the growing spherulite phase, they are expected to escalate on the surface of the growing crystal front. This in turn may consequently impede the migration of the crystallizable species from the melt phase to the growing front. This phenomenon leads to a deflection from linear spherulite growth after a certain diameter of spherulite attained. As such no deflection from linearity for growth of spherulites is noticed in the PLA–SP bionanocomposite system (Fig. 6), it can be inferred that the SP is not eliminated during the spherulite growth process. Similar results are reported for PLA–carbon nanotubes (CNT) nanocomposites by Xu et al. [55].

Conclusions

The non-isothermal cold crystallization of PLA and PLA–SP bionanocomposites was investigated by DSC analysis under different heating rates of 2.5, 5, 7.5, and 10 °C/min. The influence of SP on the cold crystallization kinetics of PLA was examined using Avrami analysis. With respect to progress in heating rate, the crystallization exotherm locates to the elevated temperature range; therefore, for both neat PLA and PLA–SP bionanocomposites, the crystallization process is enhanced. This phenomenon is further confirmed by the increasing trend obtained for ‘ K_T ’ values of Tobin model with respect to heating rate. Furthermore, the $1/t_{0.5}$ value and CRP increase with respect to SP loading that signifies an enhancement of

the crystallization rate of PLA. The ΔE values calculated using Kissinger's method are found to exhibit decreasing trend with respect to SP loadings. Increase in the nucleation density significantly with an increase of SP content (wt%) in the PLA matrix is verified by POM studies. The radial spherulite growth rate increases linearly with time, confirming that the growth rate is not dependent on the spherulite diameter.

Acknowledgments The authors sincerely thank the Department of Chemicals and Petrochemicals, Ministry of Chemicals and Fertilizers, Government of India—funded Center of Excellence for Sustainable Polymers at IIT Guwahati for research facilities to perform this work. The authors also thank Dr. David Plackett, Technical University of Denmark (DTU), Denmark for sharing bio-filler used in this study.

References

1. Yu L, Dean K, Li L (2006) Polymer blends and composites from renewable resources. *Prog Polym Sci* 36:576–602
2. Chen GQ, Patel MK (2012) Plastics derived from biological sources: present and future—a technical and an environmental review. *Chem Rev* 112:2082–2099
3. Zhang K, Mohanty AK, Misra M (2012) Fully biodegradable and biorenewable ternary blends from polylactide, poly(3-hydroxybutyrate-co-hydroxyvalerate) and poly(butylene succinate) with balanced properties. *ACS Appl Mater Interfaces* 4:3091–3101
4. Drumright RE, Gruber PR, Henton DE (2000) Polylactic acid technology. *Adv Mater* 12:1841–1846
5. Ljungberg N, Wesslen B (2005) Preparation and properties of plasticized poly(lactic acid) films. *Biomacromolecules* 6:1789–1796
6. Rasal RM, Janorkar AV, Hirt DE (2010) Poly(lactic acid) modifications. *Prog Polym Sci* 35:338–356
7. Goffin AL, Raquez JM, Duquesne E, Siqueira G, Habibi Y, Dufresne A, Dubois P (2011) From interfacial ring-opening polymerization to melt processing of cellulose nanowhisker-filled polylactide-based nanocomposites. *Biomacromolecules* 12:2456–2465
8. Bhardwaj R, Mohanty A (2007) Modification of brittle polylactide by novel hyperbranched polymer-based nanostructures. *Biomacromolecules* 8:2476–2484
9. Pan P, Liang Z, Cao A, Inoue Y (2009) Layered metal phosphonate reinforced poly(L-lactide) composites with a highly enhanced crystallization rate. *ACS Appl Mater Interfaces* 1:402–411
10. Wang S, Han C, Bian J, Han L, Wang X, Dong L (2011) Morphology, crystallization and enzymatic hydrolysis of poly(L-lactide) nucleated using layered metal phosphonates. *Polym Int* 60:284–297
11. Zhao Y, Qiu Z, Yang W (2008) Effect of functionalization of multiwalled nanotubes on the crystallization and hydrolytic degradation of biodegradable poly(L-lactide). *J Phys Chem B* 112:16461–16468
12. Yu J, Qiu Z (2011) Isothermal and nonisothermal cold crystallization behaviors of biodegradable poly(L-lactide)/octavinyl-polyhedral oligomeric silsesquioxanes nanocomposites. *Ind Eng Chem Res* 50:12579–12586
13. Mubarak Y, Harkin-Jones EMA, Martin PJ, Ahmad M (2001) Modelling of non-isothermal crystallization kinetics of isotactic polypropylene. *Polymer* 42:3171–3182
14. Liu Y, Wang L, He Y, Fan Z, Lia S (2010) Non-isothermal crystallization kinetics of poly(L-lactide). *Polym Int* 59:1616–1621
15. Park SH, Lee SG, Kim SH (2013) Isothermal crystallization behavior and mechanical properties of polylactide/carbon nanotube nanocomposites. *Compos A* 46:11–18
16. Laredoa E, Grimaub M, Belloa A, Wuc D (2013) Molecular dynamics and crystallization precursors in polylactide and poly(lactide)/CNT biocomposites in the insulating state. *Eur Polym J* 49:4008–4019

17. Wu JH, Yen MS, Kuo MC, Chen BH (2013) Physical properties and crystallization behavior of silica particulates reinforced poly(lactic acid) composites. *Mater Chem Phys* 142:726–733
18. Qian Y, Wei P, Jiang P, Li Z, Yan Y, Ji K (2013) Aluminated mesoporous silica as novel high-effective flame retardant in polylactide. *Compos Sci Technol* 82:1–7
19. Gerds N, Katiyar V, Koch CB, Risbo J, Plackett D, Hansen HCB (2012) Synthesis and characterization of laurate-intercalated Mg–Al layered double hydroxide prepared by coprecipitation. *Appl Clay Sci* 65:143–151
20. Ashabi L, Jafari SH, Khonakdar HA, Haussler L, Wagenknecht U, Heinrich G (2013) Non-isothermal crystallization behavior of PLA/LLDPE/nanoclay hybrid: synergistic role of LLDPE and clay. *Thermochim Acta* 565:102–113
21. Fortunati E, Armentano I, Zhou Q, Puglia D, Terenzi A, Berglund LA, Kenny JM (2012) Microstructure and nonisothermal cold crystallization of PLA composites based on silver nanoparticles and nanocrystalline cellulose. *Polym Degrad Stab* 97:2027–2036
22. Suryanegara L, Nakagaito AN, Yano H (2009) The effect of crystallization of PLA on the thermal and mechanical properties of microfibrillated cellulose-reinforced PLA composites. *Compos Sci Technol* 69:1187–1192
23. Cai J, Liu M, Wang L, Yao K, Li S, Xiong H (2011) Isothermal crystallization kinetics of thermoplastic starch/poly(lactic acid) composites. *Carbohydr Polym* 86:941–947
24. Zhang JF, Sun X (2004) Mechanical properties of poly(lactic acid)/starch composites compatibilized by maleic anhydride. *Biomacromolecules* 5:1446–1451
25. Valapa R, Pugazhenth G, Katiyar V (2015) Fabrication and characterization of sucrose palmitate reinforced poly(lactic acid) bionanocomposite films. *J Appl Polym Sci* 132:41320–41330
26. Valapa R, Pugazhenth G, Katiyar V (2014) Thermal degradation kinetics of sucrose palmitate reinforced poly(lactic acid) biocomposites. *Int J Biol Macromol* 65:275–283
27. Huda MS, Drzal LY, Misra M (2005) A study on biocomposites from recycled newspaper fiber and poly(lactic acid). *Ind Eng Chem Res* 44:5593–5601
28. Peng F, Shaw MT, Olson JR, Wei M (2011) Hydroxyapatite needle-shaped particles/poly(L-lactic acid) electrospun scaffolds with perfect particle-along-nanofiber orientation and significantly enhanced mechanical properties. *J Phys Chem C* 115:15743–15751
29. Liu L, Jin TZ, Coffin DR, Hicks KB (2009) Preparation of antimicrobial membranes: coextrusion of poly(lactic acid) and nisaplin in the presence of plasticizers. *J Agric Food Chem* 57:8392–8398
30. Katiyar V, Gerds N, Koch CB, Risbo J, Hansen HCB, Plackett D (2010) Poly L-lactide-layered double hydroxide nanocomposites via in situ polymerization of L-lactide. *Polym Degrad Stab* 95:2563–2573
31. Sawai D, Takahashi K, Sasashige A, Kanamoto T, Hyon SH (2003) Preparation of oriented β -form poly(L-lactic acid) by solid-state co-extrusion: effect of extrusion variables. *Macromolecules* 36:3601–3605
32. Hoogsteen W, Postema AR, Pennings AJ, Brinke GT (1990) Crystal structure, conformation and morphology of solution-spun poly(L-lactide) fibers. *Macromolecules* 23:634–642
33. Bharadwaj R, Mohanty AK, Drzal LT, Pournoghra F, Misra M (2006) Renewable resource-based green composites from recycled cellulose fiber and poly(3-hydroxybutyrate-co-3-hydroxyvalerate) bioplastic. *Biomacromolecules* 7:2044–2051
34. Ali SS, Tang X, Alavi S, Faubion J (2011) Structure and physical properties of starch/poly vinyl alcohol/sodium montmorillonite nanocomposite films. *J Agric Food Chem* 59:12384–12395
35. Ravari F, Mashak A, Nekoomanesh M, Mobedi H (2013) Non-isothermal cold crystallization behavior and kinetics of poly(L-lactide): effect of L-lactide dimer. *Polym Bull* 70:2569–2586
36. Yasuniwa M, Sakamo K, Ono Y, Kawahara W (2008) Melting behavior of poly(L-lactic acid): X-ray and DSC analyses of the melting process. *Polymer* 49:1943–1951
37. Kong Y, Hay JN (2003) Multiple melting behaviour of poly(ethylene terephthalate). *Polymer* 44:623–633
38. Fukushima K, Abbate C, Tabuani D, Gennari M, Camino G (2009) Biodegradation of poly(lactic acid) and its nanocomposites. *Polym Degrad Stab* 94:1646–1655
39. Fortunati E, Armentano I, Zhou Q, Puglia D, Terenzi A, Berglund LA, Kenny JM (2012) Microstructure and nonisothermal cold crystallization of PLA composites based on silver nanoparticles and nanocrystalline cellulose. *Polym Degrad Stab* 7:2027–2036
40. Nofar M, Zhu W, Park CB, Randall J (2011) Crystallization kinetics of linear and long-chain-branched polylactide. *Ind Eng Chem Res* 50:13789–13798

41. Pei A, Zhou Q, Berglund LA (2010) Functionalized cellulose nanocrystals as biobased nucleation agents in poly(L-lactide) (PLLA)—crystallization and mechanical property effects. *Compos Sci Technol* 70:815–821
42. Vasanthan N, Ly H, Ghosh S (2011) Impact of nanoclay on isothermal cold crystallization kinetics and polymorphism of poly(L-lactic acid) nanocomposites. *J Phys Chem B* 115:9556–9563
43. Wang L, Jing X, Cheng H, Hu X, Yang L, Huang Y (2012) Blends of linear and long-chain branched poly(L-lactide)s with high melt strength and fast crystallization rate. *Ind Eng Chem Res* 51:10088–10099
44. Wu D, Wu L, Xu B, Zhang Y, Zhang M (2007) Nonisothermal cold crystallization behavior and kinetics of polylactide/clay nanocomposites. *J Polym Sci B Polym Phys* 45:1100–1113
45. Qiu Z, Li Z (2011) Effect of orotic acid on the crystallization kinetics and morphology of biodegradable poly(L-lactide) as an efficient nucleating agent. *Ind Eng Chem Res* 50:12299–12303
46. Yi L, Han C (2012) Isothermal and nonisothermal cold crystallization behaviors of asymmetric poly(L-lactide)/poly(D-lactide) blends. *Ind Eng Chem Res* 51:15927–15935
47. Zhang R, Zheng H, Lou X, Ma D (1994) Crystallization characteristics of polypropylene and low ethylene content polypropylene copolymer with and without nucleating agents. *J Appl Polym Sci* 51:51–56
48. Wu M, Yang G, Wang M, Wang W, Zhang W, Feng J, Liu T (2008) Nonisothermal crystallization kinetics of zno nanorod filled polyamide 11 composites. *Mater Chem Phys* 109:547–555
49. Tsuji H, Sawada M, Bouapao L (2009) Biodegradable polyesters as crystallization-accelerating agents of poly(L-lactide). *ACS Appl Mater Interfaces* 1:1719–1730
50. Bao RY, Yang W, Jiang WR, Liu ZY, Xie BH, Yang MB (2013) Polymorphism of racemic poly(L-lactide)/poly(D-lactide) blend: effect of melt and cold crystallization. *J Phys Chem B* 117:3667–3674
51. Liao R, Yang B, Yu W, Zhou C (2007) Isothermal cold crystallization kinetics of polylactide/nucleating agents. *J Appl Polym Sci* 104:310–317
52. Han Q, Wang Y, Shao C, Zheng G, Li Q, Shen C (2013) Nonisothermal crystallization kinetics of biodegradable poly(lactic acid)/zinc phenylphosphonate composites. *J Compos Mater*. doi:[10.1177/0021998313502064](https://doi.org/10.1177/0021998313502064)
53. Maiti SN, Hemalatha (2012) Nonisothermal crystallization kinetics of PA6 and PA6/SEBS-g-MA Blends. *J Polym Res* 19:9926–9942
54. Li DC, Liu T, Zhao L, Lian XS, Yuan WK (2011) Foaming of poly(lactic acid) based on its nonisothermal crystallization behavior under compressed carbon dioxide. *Ind Eng Chem Res* 50:1997–2007
55. Xu Z, Niu Y, Wang Z, Li H, Yang L, Qiu J, Wang H (2011) Enhanced nucleation rate of polylactide in composites assisted by surface acid oxidized carbon Nanotubes of Different Aspect Ratios. *ACS Appl Mater Interfaces* 3:3744–3753